ELSEVIER

Contents lists available at ScienceDirect

Sustainable Cities and Society

journal homepage: www.elsevier.com/locate/scs





Quantifying the decarbonization potential of mobile heat battery in low-temperature district heating

Shuwei Wang a,*, Pieter-Jan Hoes a, Jan L.M. Hensen a, Olaf C.G. Adan b,c

- a Department of the Built Environment, Eindhoven University of Technology, Eindhoven, The Netherlands
- ^b Department of Applied Physics, Eindhoven University of Technology, Eindhoven, The Netherlands
- ^c TNO Materials Solutions, Eindhoven, The Netherlands

ARTICLE INFO

Keywords: Thermochemical heat storage District heating Waste heat recovery Building performance simulation Decarbonization

ABSTRACT

This research assesses the potential of a mobile thermochemical storage system, the mobile heat battery (M-HB), for decarbonizing a low-temperature district heating (DH) system in the Netherlands. The assessment is built on a case study where the M-HB is used to transport waste heat from different sources to a neighborhood interface of a DH system. This case study utilizes a simulation-based methodology to calculate the emissions from grid electricity, DH, and M-HB transport and charging. Building performance simulation is used as the main experimental method in combination with both empirical data and theoretical assumptions. Various system operational strategies and uncertain factors are explored, and waste heat sources are screened by different decarbonization targets. Findings indicate that using the M-HB can reduce the operational carbon emissions by up to 80 %, from approximately 60–70 KgCO₂/GJ of the system without M-HB to around 13 KgCO₂/GJ in optimal scenarios. Emissions from M-HB transport and charging are identified as more influential to the decarbonization potential than other considered factors, which addresses the significance of choosing proper waste heat sources. Despite some limitations from data availability and assumptions, this work identifies both opportunities and challenges for using M-HB to decarbonize DH systems.

1. Introduction

1.1. Low-temperature district heating and mobile thermal energy storage

The shift towards low-temperature district heating (DH) systems is essential for enhancing energy efficiency and mitigating environmental impacts (Lund et al., 2014). These systems, operating at around 45 °C to 55 °C, facilitate the integration of low-emission energy sources. However, they frequently face a mismatch between the production of low-emission heat and consumer demand, especially during peak periods. This discrepancy often leads to a reliance on high-emission backup sources to fill the gap, diminishing the system's environmental benefits. The European Emission Trading System 2 (ETS 2) extends this impact also to the economic perspective as it enables the trading of carbon emissions (European Commission, 2023). This issue exists not only in low-temperature DH systems but also in those with higher operation temperatures. The performance of existing DH networks in the Netherlands can provide some evidence.

Fig. 1 displays the annual average carbon emission and primary

Adopting energy storage is a proven approach to achieving these goals, and diverse energy storage technologies are applied in this sector including both thermal energy storage (TES) and electrochemical energy storage (Parra et al., 2017). Towards the application in heating practice, thermal energy storage stands out for its cost-effectiveness (Parra et al., 2017; Zhou & Liu, 2023). TES systems can relieve the intermittency of energy from renewable sources (Guelpa & Verda, 2019) and can play a significant role in the transition toward carbon-neural district energy communities (Zhou & Liu, 2023). The literature provides diverse cases where TES is applied to decarbonize district heating, covering large-scale seasonal configurations (Maximov et al., 2021), compact

energy factors of various DH networks in the Netherlands, with individual dots denoting distinct systems. The observed emission factors for these systems range from 6 to 130 $\rm KgCO_2/GJ$ of heat in 2021, and 5 to 125 $\rm KgCO_2/GJ$ of heat in 2022. The variation in their emission factors, as indicated by the color-coded data points, is largely influenced by the proportion of peak/backup natural gas used in the total energy mix. This underscores the significant decarbonization potential of sustainably replacing high-emission peak energy sources and effectively managing demand fluctuations.

^{*} Corresponding author: P.O. Box 513, 5600 MB Eindhoven, The Netherlands. *E-mail address:* s.wang5@tue.nl (S. Wang).

Ablr eviations API Application programming interface ef trans BPS Building performance simulation m Subscript to indicate the number of discharging strategie CU Charging unit for the mobile heat battery n Subscript to indicate the number of uncertain scenarios CV(RMSE) Coefficient of the variation of the root mean square error DH District heating DHW Domestic hot water o Operational strategy for the mobile heat battery HP Water-to-water heat pump at the substation KPI Key performance indicator q HB Heat stored in the heat battery M-HB Mobile heat battery M-TES Mobile (mobilized) thermal energy storage R Radiator groups in the buildings Soc State of charge of the heat battery Symbols COPHB, d COefficient of performance of the heat battery for discharging COPHB Coefficient of performance of the heat pump e elec Electricity consumed by the heating system Emission factor for transporting heat battery Emission factor for transporting heat battery Emission factor for transporting heat battery Emission factor for transporting heat battery in cache care to purple to indicate the number of discharging strategie Emission factor for transporting heat battery in clusted the number of dischargins strategie to indicate the number of dischargins strategie on Subscript to indicate the number of dischargins strategies the number of mobile heat battery in demonstrate to indicate the number of dischargins strategies on purple and the number of mobile heat battery Heat delivered from the substation buildings PHE Heat tored in the heat battery Heat stored in the heat battery Heat extracted from the district heating system Heat in purple of mobile heat battery Heat elivered from the deitrict heating substation OphHB, d Heat extracted from the district heating substation PHB Heat in purple of mobile heat battery Heat extracted from the constitution to purple of mobile heat battery Heat elivered from the elevature of the district heating substation OphHB, d Heat extracted from the constitution to pu	Nomenclature		ef ^{char}	ef char Emission factor for charging heat battery		
API Application programming interface BPS Building performance simulation m Subscript to indicate the number of discharging strategie CU Charging unit for the mobile heat battery n Subscript to indicate the number of uncertain scenarios $CV(RMSE)$ Coefficient of the variation of the root mean square error DH District heating DHW Domestic hot water DU Discharging unit for the mobile heat battery DU Heat extracted from the substation to buildings DU Heat delivered from the district heating DU Heat extracted from the district heating DU Heat go utput power from the heat battery DU Heat stored in the heat battery DU Heat stored in the heat battery DU Heat stored in the heat battery DU Heat ing output power from the heat pump DU Heat stored in the heat battery DU Heat ing output power from the heat pump DU Heat stored in the heat battery DU Heat stored in the heat			ef ^{DH}	Emission factor for heat from district heating		
BPS Building performance simulation m Subscript to indicate the number of discharging strategies CU Charging unit for the mobile heat battery n Subscript to indicate the number of uncertain scenarios $CV(RMSE)$ Coefficient of the variation of the root mean square error DH District heating DHW Domestic hot water DH District heating DHW Domestic hot water DH Discharging unit for the mobile heat battery DH Heat delivered from the substation to buildings DH Heat extracted from the district heating DH Heat extracted from the district heating DH Heat stored in the heat battery DH Heat stored in the heat battery DH Heat stored in the heat battery DH Heat ing output power from the heat pump DH Heating output power from the heat battery DH Heating output power from the heat pump DH Heating output power from the heat pump DH Heating output power from the heat battery DH Heating output power from the heat pump DH Heating output power from the heat battery DH Heating output power from the heat battery DH Heating output power from the heat battery DH Heating output power from the district heating system DH Heating output power from the district heating DH Heating output power from the distric		Abbreviations				
CU Charging unit for the mobile heat battery n Subscript to indicate the number of uncertain scenarios $CV(RMSE)$ Coefficient of the variation of the root mean square error DH District heating DHW Domestic hot water DU Discharging unit for the mobile heat battery DU Heat delivered from the substation to buildings DU Heat delivered from the district heating DU Heat is output power from the heat battery DU Heat stored in the heat battery DU Heat stored in the heat battery DU Heat stored in the heat battery DU Heat ing output power from the heat pump DU Heat ing output power from the heat pump DU Heat ing output power from the heat pump DU Heating output power from the heat battery DU Heating output power from the district heating DU Heating output power from the district			ef trans			
CV(RMSE) Coefficient of the variation of the root mean square error DH District heating DHW Domestic hot water O Operational strategy for the mobile heat battery O Discharging unit for the mobile heat battery O Heat delivered from the substation to buildings O Heat extracted from the district heating O Heat stored in the heat battery O Heating output power from the heat pump O Heating output power from the heat battery O Heating output power from the heat battery O Heating output power from the heat pump O Heating output power from the heat battery O Heating output power from the heat pump O Heating output power from the heat battery O Heati	BPS		m			
DH District heating substation DHW Domestic hot water o Operational strategy for the mobile heat battery DU Discharging unit for the mobile heat battery q^d Heat delivered from the substation to buildings HP Water-to-water heat pump at the substation q^{DH} Heat extracted from the district heating KPI Key performance indicator q^{HB} Heating output power from the heat battery MAPE Mean absolute percentage error Q^{HB} Heat stored in the heat battery M-HB Mobile heat battery q^{HP} Heating output power from the heat pump M-TES Mobile (mobilized) thermal energy storage R_c Thermal resistance of the construction R Radiator groups in the buildings q^{HB} Scenarios for the considered factors SoC State of charge of the heat battery q^{HB} Discharging water temperature of the district heating system TES Thermal energy storage q^{HB} Discharging water temperature Symbols q^{HB} Outdoor air temperature Coefficient of performance of the heat battery for discharging q^{HB} Supply water temperature of the substation Discharging efficiency of the heat battery Time Coefficient of performance of the heat pump q^{HB} Electricity consumed by the heating system To Start the calendar year End of the calendar year	CU	Charging unit for the mobile heat battery		Subscript to indicate the number of uncertain scenarios		
DHW Domestic hot water DU Discharging unit for the mobile heat battery HP Water-to-water heat pump at the substation KPI Key performance indicator MAPE Mean absolute percentage error M-HB Mobile heat battery M-TES Mobile (mobilized) thermal energy storage R Radiator groups in the buildings SoC State of charge of the heat battery TES Thermal energy storage COP ^{HB, d} Coefficient of performance of the heat battery for discharging COP ^{HP} Coefficient of performance of the heat pump Electricity consumed by the heating system O Operational strategy for the mobile heat battery Heat delivered from the substation to buildings q^{DH} Heat extracted from the district heating HP Heat stored in the heat battery Heat stored in the heat battery Heat stored in the heat battery Heating output power from the heat pump Full Heat stored in the heat battery Heating output power from the heat battery Heating output power from the heat battery Heat extracted from the substation PHB Heat extracted from the substation AHB Heat extracted from the district heating Heat sored in the heat battery Heat extracted from the district heating Heat sored in the heat battery Heat extracted from the district heating Heat extracted from the district heating Heat extracted from the district heating Heat sored in the heat battery Heat extracted from the district heating Heat sored in the heat battery Heat sored in the heat	CV(RMS	CV(RMSE) Coefficient of the variation of the root mean square error		The number of mobile heat batteries transported to the		
DU Discharging unit for the mobile heat battery HP Water-to-water heat pump at the substation KPI Key performance indicator MAPE Mean absolute percentage error M-HB Mobile heat battery M-TES Mobile (mobilized) thermal energy storage R Radiator groups in the buildings SoC State of charge of the heat battery TES Thermal energy storage Symbols COP ^{HB} , d Coefficient of performance of the heat battery for discharging COP ^{HB} , d COefficient of performance of the heat pump COP ^{HB} , e elec Electricity consumed by the heating system PHeat delivered from the substation to buildings q^{BH} Heat extracted from the district heating Heat extracted from the district heating sutput power from the heat battery Heating output power from the heat battery Heat extracted from the district heating sutput power from the district heating output power from the heat battery Heat extracted from the district heating output power from the heat battery Heat extracted from the district heating sutput power from the heat battery Heat extracted from the district heating output power from the heat battery Heat extracted from the district heating output power from the heat battery Heat extracted from the district heating output power from the heat battery Heat extracted from the district heating output power from the heat battery Heat extracted from the district heating output power from the heat battery Heating output power from the district heating output power from the district heating output power from the heat battery Heating output power from the district heating output power from the district heating output power from the heat battery Heating output power from the leat battery Heating output power from the substation to buildings Scenarios for the construction	DH	District heating		substation		
HP Water-to-water heat pump at the substation q^{DH} Key performance indicator q^{HB} Heat extracted from the district heating q^{HB} Heating output power from the heat battery q^{HB} Heat stored in the heat battery q^{HB} Heating output power from the heat battery q^{HB} Heating output power from the heat pump q^{HB} Heating output power from the heat battery q^{HB} Heating output power from the heat pump q^{HB} Heating output power from the heat battery q^{HB} Heating output power from th	DHW	Domestic hot water		Operational strategy for the mobile heat battery		
KPI Key performance indicator q^{HB} Heating output power from the heat battery q^{HB} Heat stored in the heat battery q^{HB} Heat stored in the heat battery q^{HB} Heating output power from the heat pump q^{HB} Heating output power from the heat battery q^{HB} Heat stored in the heat battery q^{HB} Heating output power from the heat battery q^{HB} Heating output power from the heat pump q^{HB} Heating output power from th	DU	Discharging unit for the mobile heat battery	q^{d}	Heat delivered from the substation to buildings		
KPI Key performance indicator q^{HB} Heating output power from the heat battery q^{HB} Heat stored in the heat battery q^{HB} Heat stored in the heat battery q^{HB} Heating output power from the heat pump q^{HB} Heating output power from the heat battery q^{HB} Heat stored in the heat battery q^{HB} Heating output power from the heat battery q^{HB} Heating output power from the heat pump q^{HB} Heating output power from th	HP	Water-to-water heat pump at the substation	q^{DH}	Heat extracted from the district heating		
M-HB Mobile heat battery M-TES Mobile (mobilized) thermal energy storage R Radiator groups in the buildings SoC State of charge of the heat battery TES Thermal energy storage Symbols COP ^{HB} , d Coefficient of performance of the heat battery of discharging COP ^{HP} e^{elec} COEfficient of performance of the heat pump e^{elec} COEfficie	KPI	Key performance indicator	q^{HB}	Heating output power from the heat battery		
M-TES Mobile (mobilized) thermal energy storage R Radiator groups in the buildings SoC State of charge of the heat battery TES Thermal energy storage Symbols $COP^{HB, d}$ Coefficient of performance of the heat battery for discharging $COP^{HB, d}$ Coefficient of performance of the heat pump e^{elec} Electricity consumed by the heating system Tes Thermal energy storage R_c Thermal resistance of the construction Symbols Supply water temperature of the district heating system R_c Tout Outdoor air temperature Supply water temperature of the substation R_c Time R_c Thermal resistance of the construction Supply water temperature Time Time Touth Supply water temperature of the substation Discharging efficiency of the heat battery Time Touth Supply water temperature Supply water temperature of the substation Discharging efficiency of the heat battery Time Touth Supply water temperature Supply water temperature Supply water temperature Supply water temperature of the substation Discharging efficiency of the heat battery Time Touth Supply water temperature Supply water temperatu	MAPE	Mean absolute percentage error	Q^{HB}	Heat stored in the heat battery		
M-TES Mobile (mobilized) thermal energy storage R Radiator groups in the buildings SoC State of charge of the heat battery TES Thermal energy storage Symbols $COP^{HB, d}$ Coefficient of performance of the heat battery for discharging $COP^{HB, d}$ Coefficient of performance of the heat pump e^{elec} Electricity consumed by the heating system Tes Thermal energy storage R_c Thermal resistance of the construction Symbols Supply water temperature of the district heating system R_c Tout Outdoor air temperature Supply water temperature of the substation R_c Time R_c Thermal resistance of the construction Supply water temperature Time Time Touth Supply water temperature of the substation Discharging efficiency of the heat battery Time Touth Supply water temperature Supply water temperature of the substation Discharging efficiency of the heat battery Time Touth Supply water temperature Supply water temperature Supply water temperature Supply water temperature of the substation Discharging efficiency of the heat battery Time Touth Supply water temperature Supply water temperatu	М-НВ	Mobile heat battery	q^{HP}	Heating output power from the heat pump		
SoC State of charge of the heat battery t_{DH} Supply water temperature of the district heating system TES Thermal energy storage t_{dis} Discharging water temperature t_{out} Outdoor air temperature t_{sub} Supply water temperature of the substation t_{sub} Discharging efficiency of the heat battery t_{sub} Discharging efficiency t_{sub} Discharging t_{sub} Discharging efficiency t_{sub} Discharging t_{sub} Discharging t_{sub} D	M-TES	Mobile (mobilized) thermal energy storage		Thermal resistance of the construction		
TES Thermal energy storage t_{dis} Discharging water temperature t_{out} Outdoor air temperature t_{sub} Symbols COP ^{HB, d} Coefficient of performance of the heat battery for discharging τ Coefficient of performance of the heat pump t_{out} Coefficient of performance of the heat pump t_{out} Start the calendar year t_{out} Electricity consumed by the heating system t_{out} End of the calendar vear	R	Radiator groups in the buildings	s	Scenarios for the considered factors		
TES Thermal energy storage t_{dis} Discharging water temperature t_{out} Outdoor air temperature t_{sub} Symbols COP ^{HB, d} Coefficient of performance of the heat battery for discharging τ Coefficient of performance of the heat pump t_{out} Coefficient of performance of the heat pump t_{out} Start the calendar year t_{out} Electricity consumed by the heating system t_{out} End of the calendar vear	SoC	State of charge of the heat battery	t_{DH}	Supply water temperature of the district heating system		
Symbols COP ^{HB, d} Coefficient of performance of the heat battery for discharging COP ^{HB} Coefficient of performance of the heat pump e^{elec} Electricity consumed by the heating system $e^{t_{out}}$ Outdoor air temperature t_{sub} Supply water temperature of the substation Discharging efficiency of the heat battery τ Time τ_0 Start the calendar year τ End of the calendar vear	TES	Thermal energy storage	t_{dis}			
Symbols $COP^{HB, d}$ Coefficient of performance of the heat battery for discharging τ Use τ_0 Coefficient of performance of the heat battery τ Time τ_0 Start the calendar year τ End of the calendar vear				Outdoor air temperature		
COP ^{rib, all} Coefficient of performance of the heat battery for discharging τ Uischarging efficiency of the heat battery τ Time τ_0 Start the calendar year τ End of the calendar vear						
discharging τ Time COP^{HP} Coefficient of performance of the heat pump τ_0 Start the calendar year e^{elec} Electricity consumed by the heating system τ_V End of the calendar vear	COP ^{HB, d}	Coefficient of performance of the heat battery for	n ^{HB} , d	** *		
COP^{HP} Coefficient of performance of the heat pump τ_0 Start the calendar year ϵ^{elec} Electricity consumed by the heating system ϵ^{elec} End of the calendar year		8 8	•			
e eee Electricity consumed by the heating system $ au_{v}$ End of the calendar year		Coefficient of performance of the heat pump	το	Start the calendar year		
	e ^{elec}	Electricity consumed by the heating system	· ·	· · · · · · · · · · · · · · · · · · ·		
ef Emission factor of the heating system	ef	Emission factor of the heating system	· y	and of the chemical year		

building-integrated ones (Ju et al., 2023), or a combination of both types (Pans et al., 2024). The TES systems can either be integrated into a single-source district heating system (Siddiqui et al., 2021) or be coupled with heat and power co-generation (Jokinen et al., 2022).

Building on the foundation of TES, mobilized thermal energy storage (M-TES) introduces another dimension to TES by transporting energy from such low-emission sources as industrial waste heat to the demand side, as showcased in Guo et al. (2022); Miró et al. (2016). M-TES's flexibility and adaptability make it particularly valuable for the resilient and efficient operation of DH systems (Du et al., 2021). Multiple TES technologies have been explored in this mobilized configuration, including sensible heat storage (Kuang et al., 2022), latent heat storage (Liu et al., 2022), and thermochemical ones (Zeng et al., 2023). Despite the advantages, sensible and latent heat storage systems, while common, face some limitations such as the physical properties of materials. These limitations include lower energy density and higher thermal losses, which can impact their efficiency and space effectiveness. In contrast, thermochemical storage offers higher energy density and negligible thermal losses, making it a more efficient and space-effective alternative

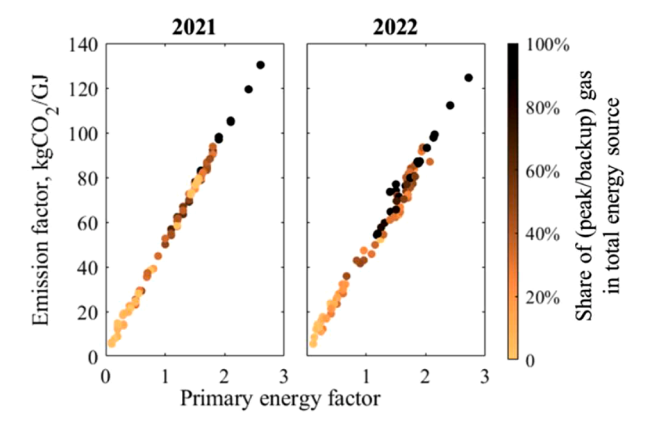


Fig. 1. Scatter plots illustrating the primary energy factor versus the emission factor of Dutch DH systems for the years 2021 (left) and 2022 (right). Data sourced from Eneco (2023); Ennatuurlijk (2023); Vattenfall (2023).

for thermal energy transportation according to Zeng et al. (2023).

1.2. Quantification under uncertainty: the research gap

As a novel technology, thermochemical heat storage has attracted widespread research interest (Yan & Zhang, 2022). At the material level, research efforts have primarily focused on enhancing the adsorption properties of adsorbents, a critical factor in improving system efficiency (Bennici et al., 2022; Xu et al., 2019). On system level, studies aim to augment the overall process of heat generation, transformation, and utilization, necessitating a broader scope that includes not only material optimization but also the design and integration of these systems (Gautam & Saini, 2020; Rouhani et al., 2019). However, there are challenges for thermochemical heat storage systems in their practical applications. A notable gap still exists in the quantitative evaluation of these systems due to their limited commercial application in DH networks and the shortcomings of existing evaluation approaches such as the high costs associated with experimental setups and the complexity of developing physics-based models. This has led to a lack of empirical data, highlighting the need for targeted research and pilot projects to explore their scalability in DH, efficiency, and cost-effectiveness (Kant & Pitchumani, 2022).

As an innovative M-TES, a mobile heat battery (M-HB) is investigated as the focus of this research because of its relatively high level of technology readiness and the availability of sufficient performance data for a quantitative evaluation. It is built on the reversible hydration of potassium carbonate (K_2CO_3) composites and encased in standard intermodal containers (Cellcius BV, 2023) as depicted in Fig. 2. The M-HB provides a storage capacity of around 10 GJ and a discharging power up to 100 kW. It has an electricity-driven mechanical system that ensures efficient and continuous thermal power for charging and discharging.

Given the crucial need to understand the potential of this type of system, this study poses a research question: How effective is the integration of a mobile thermochemical heat battery in reducing operational carbon emissions in low-temperature DH systems? This question seeks to bridge the mentioned knowledge gap and identify the possible role of thermochemical heat storage solutions in DH systems.



Fig. 2. Picture of the mobile heat battery (Cellcius BV, 2023).

1.3. Novelty and contribution

To answer the above research question, this study undertakes an exploratory case study of using the M-HB in a low-temperature DH system in the Netherlands. The main research objective is to quantify the decarbonization potential of the M-HB by mapping its functions with the practical needs of a neighborhood connected to the DH system, and the primary hypothesis of the case study is that the integration of the M-HB could reduce the operational carbon emissions from the DH system. Considering the various uncertainties and data availability, this work selects building performance simulation (BPS) as the main research method, which has been applied in district-level building energy modeling (Elci et al., 2018; Johari et al., 2023) as well as single-building-level performance assessment of a compact heat battery (Wang et al., 2023a). BPS enables the analysis of complex building energy models efficiently and economically, avoiding the high costs associated with empirical experimentation (Loonen et al., 2019). Based on the validation and verification of the models and simulation approach, the decarbonization potential of the M-HB is assessed under 12 operational strategies and 48 variant scenarios. The concept of a 'waste heat harvest circle' is proposed to encompass those waste heat sources that are theoretically feasible for the M-HB to provide the decarbonization benefit. The main contributions of this work include:

- Quantifying Decarbonization Potential: this paper provides an innovative analysis of the decarbonization potential for the novel M-HBs in the context of future DH and electricity grid scenarios. Both the proposed quantification method and the calculated operational emission factor of heating can add valuable information to the existing literature.
- Operational Strategy Assessment: The study defines and examines various operational strategies, emphasizing the importance of context in the effective use of M-HBs and providing insights essential for various stakeholders including the DH operator, heat battery developer, and waste heat supplier.
- Waste Heat Source Classification and Screening: The study geographically classifies the waste heat sources for different decarbonization targets using the waste heat harvest circle concept, highlighting opportunities for cascade utilization of the waste heat in the Netherlands and the commercial integration of M-HBs into the built environment.

The next chapter of this paper describes the case study background, addressing the target neighborhood, the potential stakeholders, and waste heat recovery possibilities in the Netherlands. Chapter 3 explains the workflow of the simulation study, including assumptions, experimental design, modeling, and simulation approach. Chapter 4 presents a verification of the simulation results and compares some data to

available benchmark values. Chapter 5 is a further analysis of the simulation outcomes to illustrate the decarbonization potential and the waste heat harvest circle. Chapter 6 includes a discussion of the methodology and a comparative analysis with other alternatives. Chapter 7 synthesizes the key findings and conclusions, providing insights into the decarbonization potential, efficient operational strategies, waste heat source selection, and implications for the further development of this technology.

2. Methodology - background analysis

2.1. Where - the target neighborhood

In the Netherlands, terraced and corner houses account for over 3 million homes, comprising approximately 42 % of the total housing stock. This prevalence makes the corresponding residential communities, typically consisting of at least three terraced houses, the most common ones in the country (Statistics Netherlands - CBS, 2023b). Therefore, this study selected such a nationally representative neighborhood to make the quantification more applicable to the whole country. Fig. 3 shows the layout of the buildings in the selected neighborhood and its composition of different households based on the demographic data from Statistics Netherlands - CBS (2023a).

The neighborhood consists of 29 post-war houses in the Dutch city of Eindhoven. The neighborhood has been included in the city's ambitious shift towards sustainable heating, as it lies within the planned district heating network powered by the local wastewater treatment plant (Municipality of Eindhoven, 2023). These buildings have been renovated to improve energy efficiency, as documented by Woonbedrijf and BAM Wonen (2021). Historically reliant on gas boilers for heating, the residences had a yearly natural gas consumption exceeding 1300 m³ before the renovation (Statistics Netherlands - CBS, 2023a), with no post-renovation data for this specific neighborhood available. The potential influence of this data gap is discussed in the result chapter. However, recent average data of the whole city still suggest continued high gas usage, highlighting the critical role this neighborhood plays in demonstrating effective decarbonization strategies within the country's energy transition efforts.

2.2. Who - stakeholders

Various stakeholders may benefit from the decarbonization, including the municipality, DH operators, waste heat suppliers, homeowners, and heat battery developers. The municipality is keen on promoting innovative, sustainable energy solutions and can support

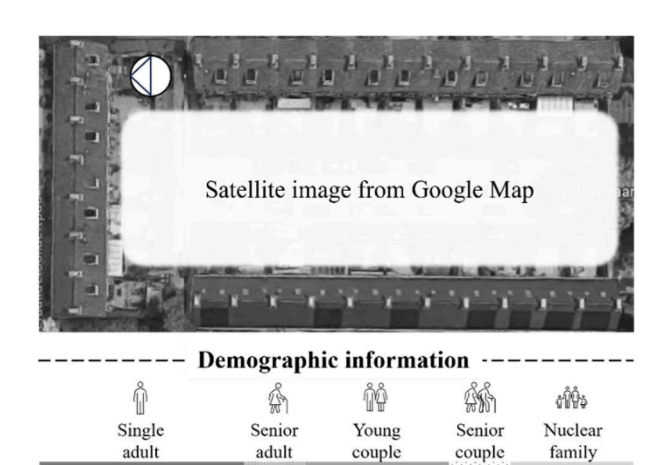


Fig. 3. Satellite image and demographic information of the selected neighborhood.

projects through policy incentives. DH operators need to integrate reliable and cost-effective heat sources, focusing on maintaining system efficiency and customer satisfaction. Industrial waste heat suppliers aim to efficiently utilize waste heat, thereby enhancing their sustainability profile and potentially benefiting from incentives or avoiding penalties. Homeowners seek affordable, sustainable heating with minimal disruption, and their collective acceptance is crucial. Heat battery developers aim to demonstrate their technology's effectiveness, seeking market opportunities and driving sustainable energy storage innovation. The common interest of all mentioned stakeholders is to reduce the carbon emissions from the heating sector in this neighborhood while minimizing cost and disruption.

2.3. How - waste heat recovery

Transporting waste heat to the target neighborhood holds promise for reducing its heating system's carbon emissions, with the available heat sources across the Netherlands considered. Fig. 4 reveals that waste heat sources with temperatures over 70 °C appear in almost every Dutch province. Two prominent clusters of waste heat sources are located near the port in Rotterdam and along the River Maas in Limburg. These clusters are approximately 100 km away from the targeted neighborhood in Eindhoven when measured by road.

However, as the size and shape of the dots in Fig. 4 denote, there are still many sources with no specific thermal power reported (squares in the map). Even those reported ones do not include sufficient information to construct a waste heat profile for further calculations. Therefore, this study defines some assumptions on waste heat supply patterns, based on existing data, with an in-depth explanation available in the methodology.

3. Methodology - simulation study

To quantify the decarbonization potential of transporting waste heat to the target neighborhood by M-HBs, this study conducts a series of experiments and analyses with specific boundary conditions, dependent

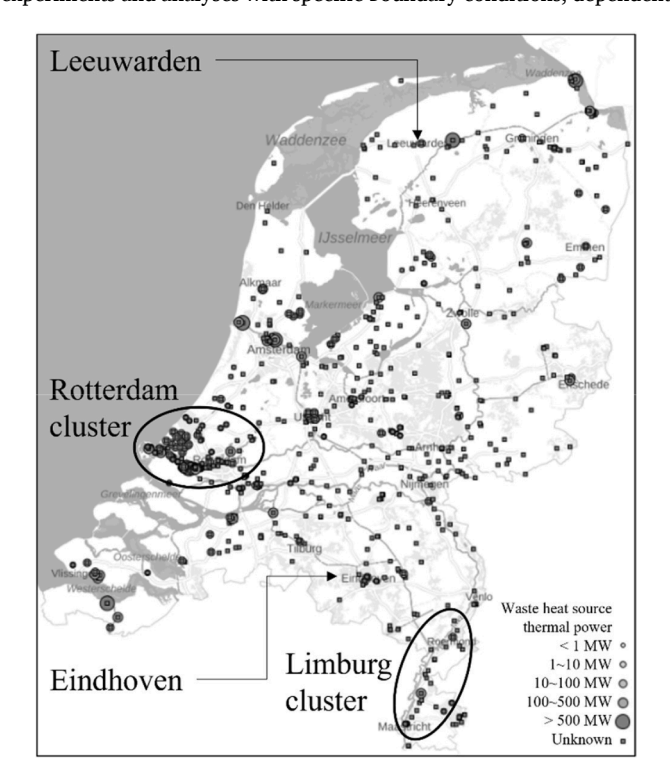


Fig. 4. Distribution of waste heat source (≥ 70 °C) in the Netherlands reported in the *Warmte Atlas* (Rijksdienst voor Ondernemend Nederland - RvO, 2023).

variables, and independent variables. The boundary conditions for these experiments are controlled and grounded in actual data and rational assumptions. The potential is quantified using a key performance indicator (KPI), which is dependent on several inputs reflecting the possible independent variations within and external to the system. Given the large scale of variations, building performance simulation is used as the main experimental method. It is both time-efficient and cost-effective, allowing for the analysis of complex interactions over extended periods without the impracticalities and expense of real-world experimentation (Loonen et al., 2019; Pan et al., 2023).

Fig. 5 presents the methodological framework and calculation scope of this simulation study. There are three steps for calculating and analyzing the KPI, namely pre-processing & experimental design, modeling & simulation, and post-processing & analysis. The first step, pre-processing & experimental design, involves gathering data from literature or stakeholder communication and defining the dependent variables, independent variables, and controlled conditions for the experiments. Secondly, in the modeling & simulation step, the performance models of the buildings, M-HB, and the DH system are constructed, validated, and implemented in BPS. Based on verified simulation outcomes, the third step, post-processing & analysis, evaluates the calculated KPI values within the defined assumptions and delivers the estimated potential to support the decision-making.

The KPI is derived from literature review and stakeholders' common interest mentioned in 2.2. It quantifies the total system's operational carbon emissions (per GJ delivered heat) from consuming grid electricity, consuming heat from DH, plus the emissions from transport and charging of the M-HB, as shown in the green area of Fig. 5. This green area denotes the scope of carbon emissions that are included in the calculation. The product carbon footprint of the M-HB is not included due to current limitations in accurately quantifying the emissions associated with its production and lifecycle. The KPI is calculated by this formula:

$$ef_{m,n} = \int_{\tau_0}^{\tau_y} \frac{ef_n^{elec}(\tau)e_{m,n}^{elec}(\tau) + ef_n^{DH}(\tau)q_{m,n}^{DH}(\tau) + \left(ef_n^{trans} + ef_n^{char}\right)n_{m,n}^{HB}(\tau)}{q_{m,n}^d(\tau)}d\tau$$

$$(1)$$

The total system's emission factor $ef_{m,n}$ (kgCO₂/GJ heat) reflects the heating system's emissions under operational strategy m and scenario n. Time is denoted by τ , with τ_o and τ_y as the start and end of the year, respectively. Emission factors ef^{elec} , ef^{DH} , ef^{trans} , and ef^{char} (kgCO₂/MWh electricity,KgCO₂/GJ heat, kgCO₂ per heat battery) represent emissions related to grid electricity, consumed heat from DH, battery transport, and charging emissions. Energy variables e^{elec} , q^{DH} , and q^d (electric or heating powers in MW) capture the heating system's electricity consumption rate, DH thermal rate, and neighborhood heat consumption rate (MW), while n^{HB} counts the heat batteries used annually.

3.1. Assumptions and design of experiments

As formula (1) indicates, the calculation of $ef_{m,n}$ requires information that is not directly dependent on the neighborhood (ef^{elec} , ef^{DH} , ef^{rans} , and ef^{char}), and outputs from the neighborhood's model of energy consumption (e^{elec} , q^{DH} , q^d , and n^{HB}). Assumptions are necessary for completing this calculation. These assumptions are based on the data availability introduced in the background part.

3.1.1. Boundary conditions

As stated by Lund et al. (2014), one of the development trends for future DH is its integration with smart electricity grids, potentially through centralized heat pumps (HP). The electricity consumed by the HP can cause carbon emissions if it is imported from the grid. In the Netherlands, there is a platform, CO_2 Monitor (NetAnders, 2023), which computes and disseminates the emission factor for the electricity mix within the Dutch power grid.

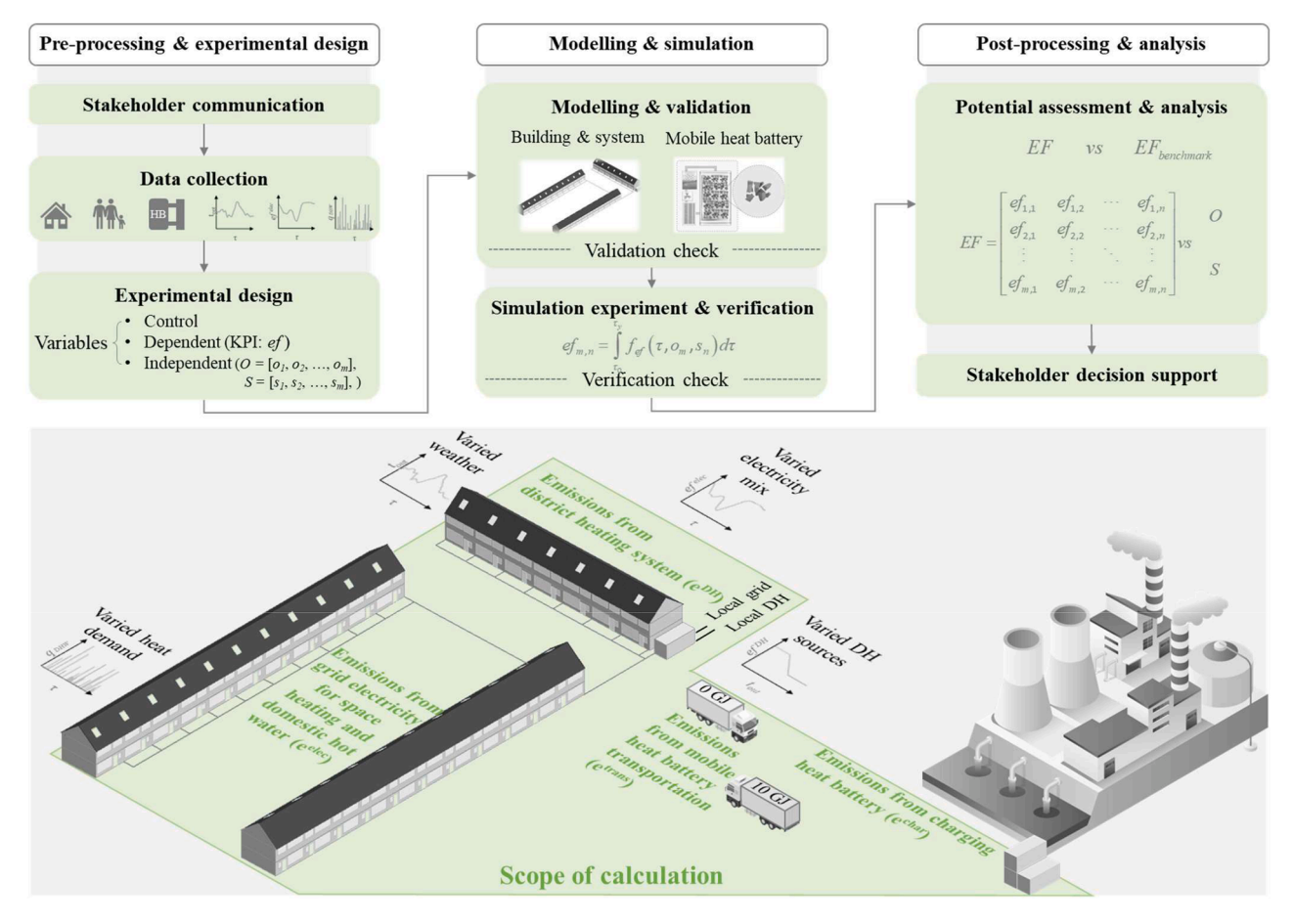


Fig. 5. Methodology and scope of the simulation study.

Fig. 6 showcases the time series data for the years 2021 and 2022 acquired from the platform. Notably, this emission factor exhibits significant fluctuations, ranging from 100 to over 400 KgCO $_2$ /MWh of electricity annually, and demonstrates obvious seasonal and diurnal patterns. These patterns result from the variable contributions of renewable energy sources, such as solar and wind, to the overall electricity production. This study employs hourly time series of e^{gelec} (for both 2021 and 2022) as presented in Fig. 6, creating two distinct scenarios. These are further combined with location-specific weather data,

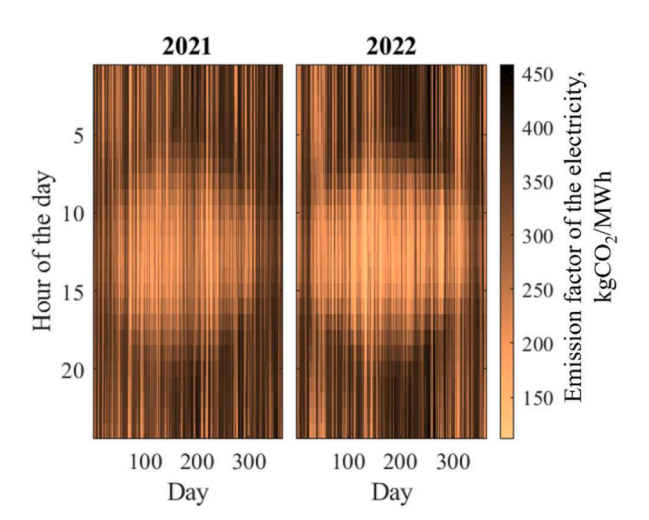


Fig. 6. Hourly emission factor of the electricity mix in the Netherlands in 2021 and 2022 (NetAnders, 2023).

resulting in four scenarios: **Eindhoven 2021, Leeuwarden 2021, Eindhoven 2022, and Leeuwarden 2022** as illustrated by the violin plot in the (a) part of Fig. 7. This division accounts for both yearly variations in the electricity mix and weather pattern differences between the northern and southern regions of the Netherlands. Weather data is

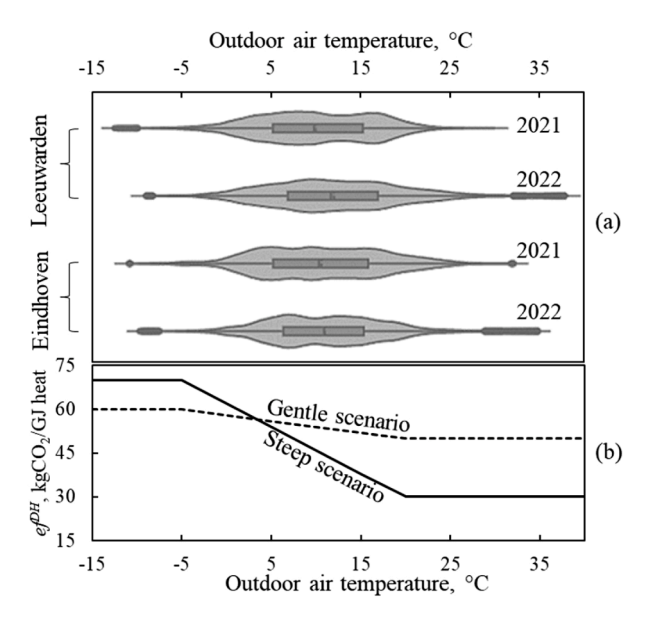


Fig. 7. Scenarios of (a) weather pattern (violin plot below shows the hourly data) and (b) assumed emission factor for DH (ef^{DH}) as functions (line graph above) of outdoor air temperature.

sourced from Koninklijk Nederlands Meteorologisch Instituut - KNMI (2023).

Due to the absence of DH emission factor data with hourly resolution, this case study utilizes the yearly values in Fig. 1 as a reference for numerical ranges and the trend lines introduced by Averfalk et al. (2023). The e_i^{DH} is modeled as temperature-dependent, accounting for increased emissions from gas boilers during colder peak times. The line graph in the (b) part of Fig. 7 illustrates two scenarios: a 'steep' scenario assumes a clean primary heat source with significant e_i^{DH} increases from peak-shaving gas boilers, and a 'gentle' scenario assumes a dirtier primary source with a lesser impact from peak-shaving.

The e^{frans} and e^{fchar} are largely influenced by the waste heat source and its location. Transportation of a M-HB might cause approximately $10~{\rm KgCO_2}$ for a $20~{\rm km}$ electric train round-trip (considering a 20-ton heat battery) based on the data from Klein et al. (2021); or $400~{\rm KgCO_2}$ for a $100~{\rm km}$ diesel truck round-trip. This study treats waste heat as emission-free, but charging the heat battery consumes electricity. Charging emissions vary: roughly $20~{\rm KgCO_2}$ under ideal conditions (high charging temperature for around $20~{\rm charging}~{\rm COP}$, and low grid electricity emissions as $e^{felec} \approx 150~{\rm KgCO_2/MWh}$) or $100~{\rm KgCO_2}$ with less favorable conditions (charging $COP \approx 10$, and high grid electricity emissions as $e^{felec} \approx 350~{\rm KgCO_2/MWh}$). To account for these uncertainties, two scenarios are posited: a ' $30/{\rm HB}$ ' scenario ($e^{frans} + e^{fchar} = 30~{\rm KgCO_2}$ per battery) and a ' $500/{\rm HB}$ ' scenario ($e^{frans} + e^{fchar} = 500~{\rm KgCO_2}$ per battery).

3.1.2. Neighborhood assumptions

The renovation of the buildings in the targeted neighborhood is assumed to increase their insulation level to the R_c value of 2.5 m² K/W as described in Wang et al. (2023b). Assumptions of occupant behavior for consuming heat are based on statistics from different datasets. The household types are derived from the demographic data of the selected neighborhood as shown in Fig. 3 (Statistics Netherlands - CBS, 2023a). Space heating thermostat setpoints are established from the WoON 2018 dataset (Ministerie van Binnenlandse Zaken en Koninkrijksrelaties (BZK) and Centraal Bureau voor de Statistiek (CBS), 2019) and profiles clustered by Luyi Xu (personal communication in 2023). Moreover, domestic hot water consumption profiles are generated using the SIM-DEUM tool whose applications are comprehensively summarized by Blokker et al. (2017). This study defines three scenarios of heat consumption in this neighborhood: low-demand, base-demand, and **high-demand scenarios.** In the base-demand scenario, different types of households use different thermostat profiles and hot water patterns. Households of single seniors or senior couples are assumed to have higher consumption than those of single adults or young couples. In the other two scenarios, heat consumption consistently varies, either higher or lower for all households.

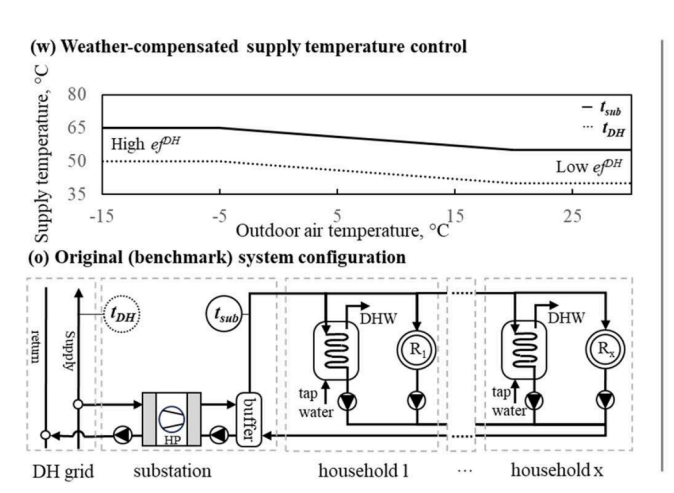
The neighborhood is assumed to be heated by the heating system presented in Fig. 8. For simplification and clarification, details such as valves and bypasses have been removed from this figure. There are three main sectors in the system, namely the DH grid, the substation, and the building systems in each household. The DH grid operates based on a weather-compensated strategy with its supply temperature adjusted based on outdoor air temperature (Averfalk et al., 2023). The substation follows the same trend but contains a water-to-water heat pump to boost the temperature for domestic hot water preparation. The M-HB is charged by the waste heat source where a charging unit is integrated into the industrial process for capturing heat. A fully charged heat battery is then transported to the neighborhood where a discharging unit is plugged into the substation allowing the heat battery to release heat upon discharging signal. The plugged M-HB can either preheat the water for the HP or completely bypass the HP to supply heat independently. The charging and discharging of the heat battery follow designated strategies as shown in Table 1.

The defined operational strategies ($o_1 \sim o_{12}$) of the M-HB cover the combinations of 2 supply patterns and 6 discharging modes. The M-HB is assumed to be supplied whenever the one plugged into the substation is empty ($o_1 \sim o_6$) or only at the start of each week ($o_7 \sim o_{12}$). Discharging is triggered by either ef^{ele} to minimize CO₂-intensive electricity use ($o_1 \sim o_3$, $o_7 \sim o_9$), or t_{out} to manage peak loads in cold periods and support heat pumps in warm periods ($o_4 \sim o_6$, $o_{10} \sim o_{12}$).

Table 1Operational strategies for supplying and discharging the M-HB.

Strategy	Supply at	Discharging when*
01	Anytime	$ef^{ele} > 200$
o_2	Anytime	$ef^{ele} > 300$
03	Anytime	$ef^{ele} > 400$
04	Anytime	$(t_{out} < 5)$ or $(t_{out} > 10)$
05	Anytime	$(t_{out} < 0)$ or $(t_{out} > 15)$
06	Anytime	$(t_{out} < -5)$ or $(t_{out} > 20)$
07	Monday 0AM	$ef^{ele} > 200$
08	Monday 0AM	$ef^{ele} > 300$
09	Monday 0AM	$ef^{ele} > 400$
010	Monday 0AM	$(t_{out} < 5)$ or $(t_{out} > 10)$
011	Monday 0AM	$(t_{out} < 0)$ or $(t_{out} > 15)$
012	Monday 0AM	$(t_{out} < -5)$ or $(t_{out} > 20)$

 $^{^*}$ precondition: buffer tank temperature \langle t_{sub} and state-of-charge of the plugged heat battery \rangle 0 %.



(p) Proposed system configuration with mobile heat battery integration

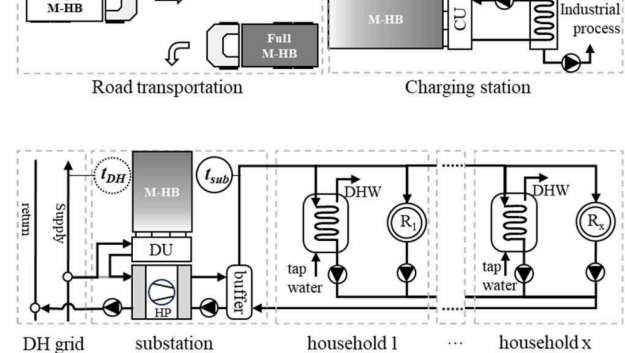


Fig. 8. Schematic representation of the system configuration with (p) and without (o) M-HB integration, and the control (w) of their supply temperature. (t_{DH} : supply temperature of the DH grid; t_{sub} : supply temperature of the substation; e_t^{DH} : emission factor of the heat from the DH system; M-HB: mobile heat battery; CU: charging unit; DU: discharging unit; HP: water-to-water heat pump; DHW: domestic hot water consumption; R: radiator group).

3.1.3. Experimental design

The variants in all aspects listed in Table 2 result in 48 combined scenarios ($s_1 \sim s_{48}$). For instance, s_1 is the combination of Eindhoven 2021, steep, low-demand, and 30/HB. In each scenario, the operational strategies ($o_1 \sim o_{12}$) from Table 1 are applied, necessitating a minimum of 576 individual simulation runs for the system integrating the heat battery. Additionally, the original system configuration (without the heat battery) is examined for benchmarking, using assumptions aligned with all combined scenarios excluding those related to the heat battery's emissions (24 in total). Consequently, the study encompasses a total of at least 600 (576+24) simulations to comprehensively investigate the outlined setup. Initially, 24 simulations for the system without the heat battery are conducted to both test the experimental method and establish KPI benchmarks. Subsequently, the remaining 576 experiments are carried out to quantify the decarbonization potential and analyze the underlying assumptions.

3.2. Modeling and simulation approach

3.2.1. Modelling and validation

To calculate the system's operational emissions, the q^{DH} and q^d can be directly taken as outputs of the simulations whereas e^{elec} and n^{HB} need extra calculations:

$$e^{elec}(\tau) = \frac{q^{_{IP}}(\tau)}{COP^{_{IP}}(\tau)} + \frac{q^{_{IB}}(\tau)}{COP^{_{IB,d}}(\tau)} + e^{_{GILX}}(\tau) \tag{2}$$

$$q^{HB}(au) = \eta^{HB,d}(au) \cdot \frac{dQ^{HB}(au)}{d au}, 0 \le Q^{HB} \le 10GJ$$
 (3)

$$n^{HB} = \left[\int_{\tau_0}^{\tau_y} \frac{q^{HB}(\tau)}{\eta^{HB,d}(\tau) \cdot 10GJ} d\tau \right] \tag{4}$$

The electricity consumption comes from the water-to-water heat pump, the discharging unit of the heat battery, and other auxiliary equipment like the pump, as explained in (2). q^{HP} and q^{HB} are the heating output powers of the heat pump and heat battery. COP^{HP} and $COP^{HB,d}$ are the coefficient of performance for the heat pump and for discharging the heat battery. e^{aux} denotes the electric power of auxiliary equipment. The heat discharged from the plugged heat battery (q^{HB}) is calculated based on a discharging efficiency ($q^{HB,d}$) and the change of thermal energy stored in the heat battery (Q^{HB}), as described by (3). The number of yearly-consumed M-HB is calculated based on the discharging of every plugged heat battery according to (4). The COP of the heat pump (COP^{HP}) is calculated with an equation-fit model in Design Builder's library, as illustrated in Fig. 9.

The heat battery's developer created a detailed first principle model based on lab experiments, which is capable of predicting various state variables using inputs like porosity and air pressure. Although accurate, this model is computationally expensive. This work trained a surrogate neural network model with the first principle model for the discharging process, and optimized it for use with BPS tools. This model inputs fluid temperature, mass flow rate, and targeted discharging power, and outputs discharging temperature (t_{dis}), discharging COP ($COP^{HB,d}$) and efficiency ($\eta^{HB,d}$).

The training process of this neural network is similar with (Wang et al., 2023a), but this study updated the training data that fit the

Table 2 Variants of mentioned scenarios.

Weather and ef ^{elec}	ef^{DH}	Heat consumption	$ef^{trans} + ef^{char}$
Eindhoven 2021	Steep	low-demand	30/HB
Eindhoven 2022	Gentle	base-demand	500/HB
Leeuwarden 2021		high-demand	
Leeuwarden 2022			

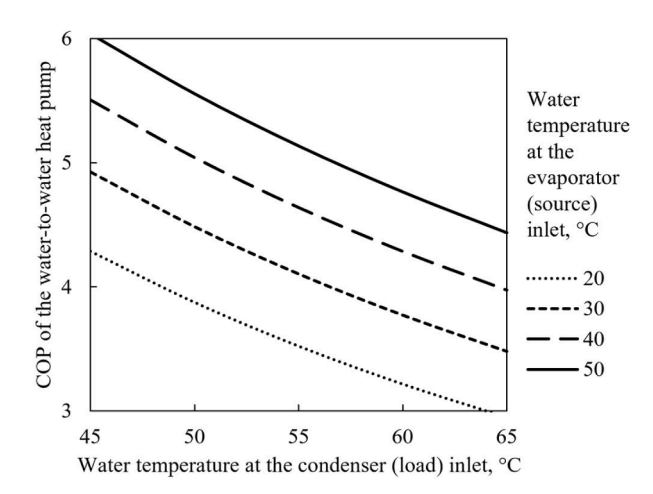


Fig. 9. Curves of equations for modeling the water-to-water heat pump in this study.

M-HB's scale and trained it with TensorFlow and Keras in Python. Table 3 provides a comparison of the prediction accuracy and the validation criteria via the index of Coefficient of the Variation of the Root Mean Square Error CV(RMSE) and Mean Absolute Percentage Error - MAPE. The neural network is validated to predict the t_{dis} $COP^{HB,d}$, η^{HB} , d with acceptable accuracy according to the criteria in (Ruiz & Bandera, 2017; Swanson, 2015).

The models for calculating space heating and domestic hot water in each house are based on the previously stated neighborhood assumptions. Space heating is simulated using a thermostat setpoint schedule that varies between 15 and 20 $^{\circ}$ C in different scenarios. Domestic hot water consumption is modeled using daily profile libraries tailored to each household type, with an average usage of about 40 liters per occupant per day in the base scenario, in line with (NEN, 2023). These models are validated by comparing the simulated heating demand with actual statistics and solid literature information.

3.2.2. Simulation and verification

To undertake the 600 simulations required by this case study, the open-source tool EnergyPlus was chosen for its flexible application programming interface (API) and the efficient multi-processing capabilities with Eppy. Fig. 10 presents the systematic framework set up for running parallel EnergyPlus simulations each day, which integrates customized plugin models. The DHW profile is updated daily using a random selection from the predefined library, ensuring varied daily usage patterns. The heat battery's integration into EnergyPlus is achieved through the PlantComponent: UserDefined object, which simulates the discharging heat exchanger's operation. Python scripts developed from EnergyPlusPlugin classes are employed to manage the discharging process's energy balance and control logic, thereby effectively capturing the heat battery's dynamics in the building energy model.

To verify the framework, multiple test runs were executed to check key outcomes such as room air temperature, domestic hot water supply temperature, heat battery performance, and the implementation of various operational strategies. These checks ensured the model's reliability in simulating actual building conditions and the effective

Table 3Test set prediction accuracy and criteria.

Index	t_{dis}	$\eta^{HB,d}$	$COP^{HB,d}$	Criteria
CV(RMSE)	0.1 %	2.3 %	6.2 %	15.0 %*
MAPE	0.1 %	3.5 %	2.7 %	5.0 %**

^{*} from Ruiz and Bandera (2017).

^{**} from Swanson (2015).

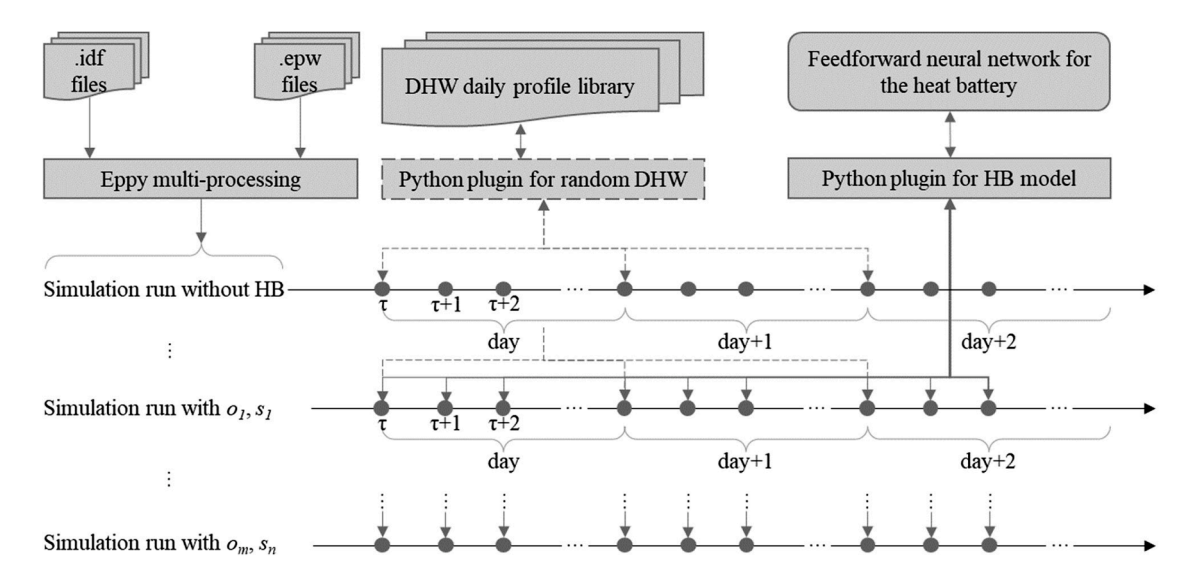


Fig. 10. Framework for parallel EnergyPlus simulations with plugin models.

integration of the heat battery system.

4. Results - verification and comparison to the benchmark

To ensure the operational strategies were correctly implemented, a period with significant fluctuations in ef^{elec} and t_{out} was analyzed, as depicted in Fig. 11. The discharging periods, highlighted by the light green area and bounded by the discharging threshold and signal, indicate when the heat battery was activated to offset carbon emissions from other sources. These periods align with the thermal energy contributions from each source at the substation, and the heat delivery pattern mirrors the neighborhood's demand, with peaks during nighttime and lower levels during the day, confirming the strategies' effective execution. The discharging frequency accurately reflects the different operational strategies but is also influenced by the heat battery's supply pattern.

Fig. 12 further substantiates the difference between continuous and weekly supply patterns, with the latter's influence evident in the sharp increases in State-of-Charge (SoC) when the battery is changed. During colder periods, the necessity for the heat battery is pronounced, but the weekly supply (o_9) effectively reduces the number of batteries used (n^{HB}) as intended. Over the year, this pattern (o_9) results in reducing the

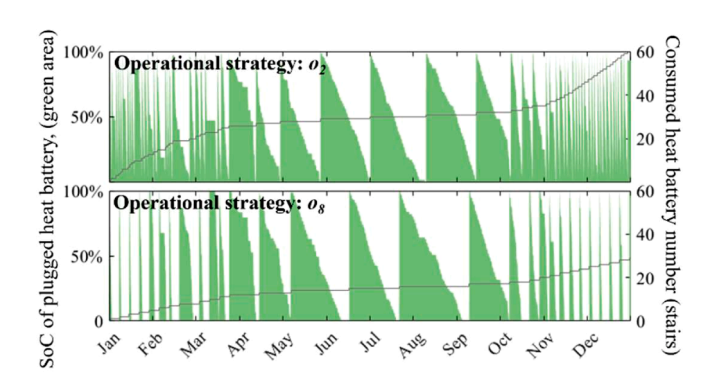


Fig. 12. Annual State-of-Charge (SoC) fluctuations (green area) and accumulated consumption count (grey lines) of the M-HB at the substation under continuous (o_2) and weekly (o_8) supply operations (related scenarios: Eindhoven 2021 and base demand).

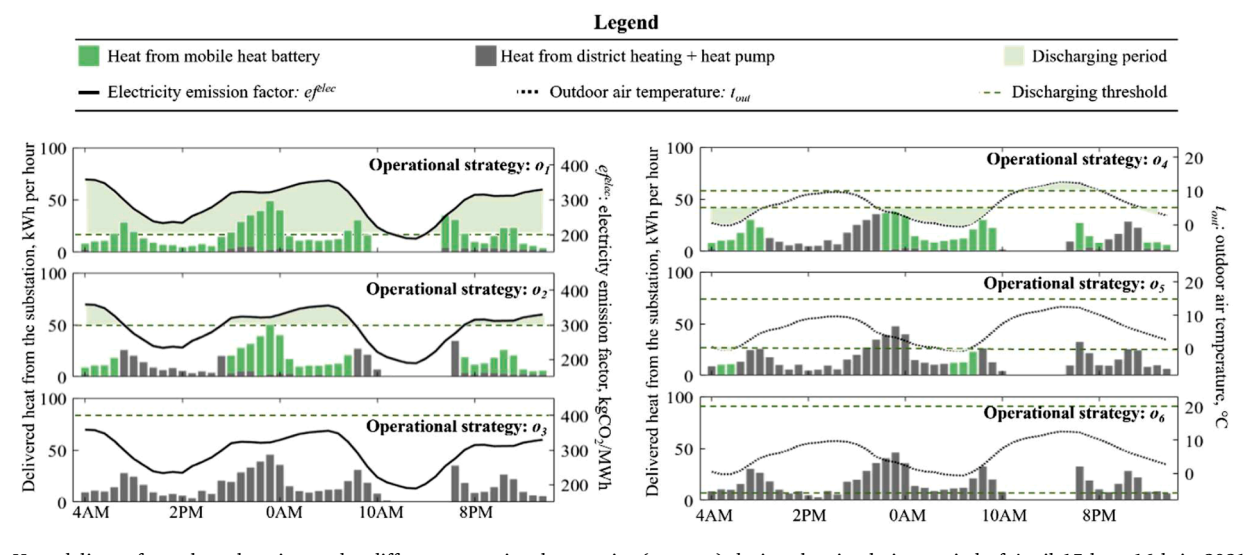


Fig. 11. Heat delivery from the substation under different operational strategies (o_1 to o_6) during the simulation period of April 15th to 16th in 2021 (related scenarios: Eindhoven 2021 and base demand).

transport frequency compared to the continuous supply (o_3) , confirming the effective and correct implementation of the operational strategies in the simulation.

For the system without M-HB integration, the annual heat consumption intensity is calculated based on the simulation results. As Fig. 13 presents, the heat consumed for space heating and DHW is around 50 to over 100 kWh per square meter floor area per year, and it varies on the weather, building types, and demand scenarios. These simulation results were benchmarked against regional statistics and a national survey for validation. The Dutch Central Agency for Statistics (Statistics Netherlands - CBS, 2023b) reports that corner houses in Leeuwarden and Eindhoven consumed above 1400 m³ of gas in 2021, and over 1100 m³ in 2022, while mid-terraced houses consumed 1250 m³ and 990 m³ in these two years. Assuming 10 m³ of gas per occupant for cooking (Boris van Beijnum & Ruud van den Wijngaart, 2023) and 95 % boiler efficiency, the heat consumption intensity for a corner house is estimated at 125 kWh/(m²·year) in 2021, and 100 kWh/(m²·year) in 2022. Similarly, a mid-terraced house's intensity is calculated at 110 kWh/(m²-year) in 2021 and 85 kWh/(m²-year) in 2022. These figures form an upper boundary for the simulation results in Fig. 13, which is logical given the difference in insulation levels between the current housing stock and the renovated neighborhood.

The national survey of WoON 2012 (Ministerie van Binnenlandse Zaken en Koninkrijksrelaties, 2014) also provide some reference values, indicating a range between 35 and 190 kWh/(m²·year) for renovated terraced houses built in similar years to those in this case study. The boxplot in Fig. 13 illustrates this range and covers all the data points from simulation outcomes. However, the data in this survey is from over 10 years ago and the 2018 version does not provide precise energy consumption figures. Consequently, the median of the boxplot is relatively higher than all simulation outcomes, which can be explained by increasing gas prices, changing climate, and other factors. This difference also aligns with the trend of heating degree days in the Netherlands. Data from the International Energy Agency (IEA, 2022) indicates a general downward trend in heating degree days (with a reference temperature of 16 $^{\circ}\text{C})$ from the survey period of WoON 2012 to the years 2021 and 2022. Table 16 in (NEN, 2017) provides annual specific heat demands of approximately 70 kWh/(m²·year) for corner houses and 40 kWh/(m²·year) for terraced houses. Though calculated under specific conditions and not intended for precise validation, they can offer a lower boundary for Fig. 13.

The simulation results for domestic hot water consumption lead to a level between 35 and 50 liters hot water per person per day, with assumed low/base/high demand scenarios reflected as shown in Fig. 14. (NEN, 2023) cites about 40 liters per person per day for hot water consumption, aligning with the simulation results in Fig. 14. This value compiles daily data from simulation experiments across various weather

Heat consumption intensity (space heating + DHW), kWh/(m² year)

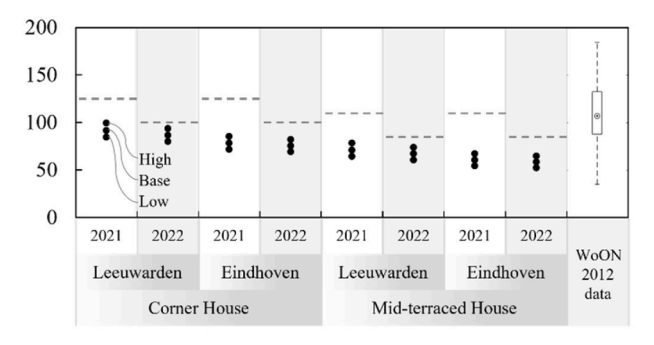


Fig. 13. Simulation results for the heat consumption intensity of the buildings in this neighborhood, where dashed lines are benchmark values based on data from Statistics Netherlands - CBS (2023b) and boxplot based on data from Ministerie van Binnenlandse Zaken en Koninkrijksrelaties (2014).

Daily hot water consumption for DHW, L / (day · occupant)

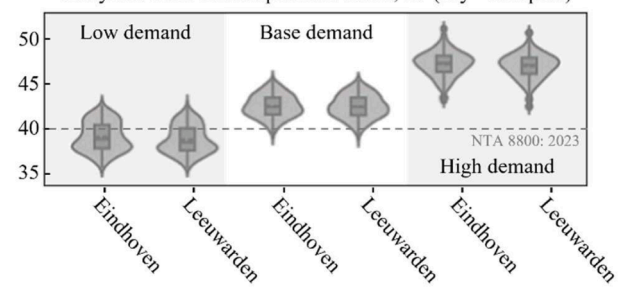


Fig. 14. Simulation results for daily hot water consumption for preparing DHW in multiple scenarios (Eindhoven/Leeuwarden, 2021/2022, low/base/high demand), where the dashed line is the average benchmark value in (NEN, 2023).

and consumption scenarios, supporting the validity of the consumption model employed in the simulations. The low, base, and high demand scenarios were distinctly differentiated as anticipated, further affirming the model's reliability.

5. Results - the decarbonization potential

5.1. The potential and its sensitivity to key assumptions

Fig. 15 presents the simulation results of the M-HB's decarbonization potential under various operational strategies, differentiating between 30/HB and 500/HB scenarios. The figure displays ridgeline plots that represent the distribution of emission factor values for each strategy. These ridgelines are ordered according to their deviation from the benchmark, which is the system operating without the heat battery. As the bottom part of Fig. 15 shows, strategies o_1 , o_2 , and o_4 are notable for their significant influence on the emission factor: they reduce emissions by up to 80 % in the 30/HB scenario, but cause an increase of about 10 % in the 500/HB scenario. The $e\!f$ is generally more sensitive to the operational strategy in 30/HB scenario than in 500/HB scenario. These two scenarios represent the extreme possibility of charging and

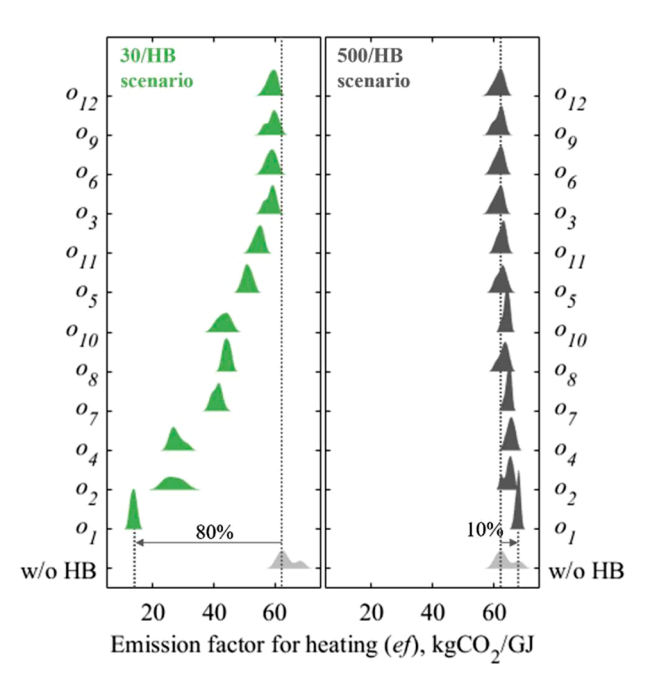


Fig. 15. Ridgeline plots comparing the emission factor (*ef*) of the system without heat battery (w/o HB) and the system with heat battery under all defined operating strategies ($O = [o_1, o_2, o_3, ..., o_{12}]$).

transportation emissions, so the ef is very likely to be enveloped by the range between them and tends to be lower than the benchmark considering the general trend. This impact is linked to the high discharging frequency and continuous waste heat supply in these strategies, as previously detailed in Fig. 11. However, the frequent transportation and replacement of the M-HB could potentially be disruptive to the local community. Therefore, it is important to consider the emission factor in relation to the number of times the M-HB (n^{HB}) is transported, which is analyzed in the next paragraph.

Fig. 16 presents the decarbonization potential of the M-HB together with the number of round-trips, and it shows how sensitive the ef is to various assumptions. As the top-left and bottom-left parts of Fig. 16 display, the emission factor associated with charging and transportation is the most significant determinant of decarbonization potential, standing out from other factors. The 30/HB and 500/HB scenarios exhibit opposing trends in emission factor changes when the number of heat battery transportations (n^{HB}) increases, suggesting a threshold value for the effectiveness of decarbonization through M-HB use. The 'steep' and 'gentle' scenarios, which represent different emission levels from DH, do not alter the outcomes significantly in any trend, implying that this factor may be of minor importance or that the range of assumptions may be too narrow to detect an effect. Additionally, scenarios considering varying heat consumption patterns and weather conditions show that greater heat demand-caused by either colder weather or intensive consumption habits—leads to increased transportation (n^{HB}) but does not necessarily enhance or diminish the decarbonization potential.

5.2. Waste heat harvest circles

Given the importance of the charging and transportation emissions identified above, a further exploration of this factor is done. Between the 30/HB and the 500/HB scenarios, two more scenarios for charging and transportation emissions are added, namely the 180/HB and the 360/HB scenarios.

Fig. 17 shows the calculated heating emission factor with a theoretical circle, the diameter of which is derived from the assumed *ef* arans reference values divided by reference values for three different transportation modalities. The radius of the circle represents the direct-line distance, rather than the actual travel distance, between the neighborhood and each potential waste heat source, delineating the feasible area

for waste heat capture. For example, an ef^{trans} of 160 KgCO₂/HB and a transportation emission of 0.2 KgCO₂/(ton·km) equate to a 20 km radius, implying a corresponding round-trip distance of 40 km for waste heat recovery. The circles in each map denote different levels of carbon emissions associated with charging and transporting a M-HB within this range, and each map represents a specific means of transportation.

When transportation results in emissions of approximately 0.2 KgCO₂/(ton·km), equivalent to emissions from diesel trucks (Klein et al., 2021), the 30/HB scenario yields a circle with a 1.3 km radius, which encompasses virtually no waste heat sources. This scenario is visually represented by a small green circle in the leftmost map. A 180/HB scenario, indicated by the larger light green circle on the same map, shows a modest increase in the area covered, including a few additional waste heat sources near the neighborhood. Conversely, in the 500/HB scenario, the incorporation of a heat battery within the neighborhood appears to negate the decarbonization benefits, as the light grey circle nearly marks the limit of where this technology remains feasible.

Changing the transportation method to a combination of electric trains and diesel trucks expands the radius for each scenario, as shown by the middle map in Fig. 17. Under these conditions, the 360/HB scenario becomes viable for accessing some waste heat sources, particularly those proximal to the River Maas and the Port of Rotterdam. Shifting entirely to transportation via electric trains would substantially widen the radius, as illustrated by the large light green circle on the rightmost map, which would then encompass waste heat sources distributed throughout the entire country.

6. Discussion

6.1. Limitations in method, assumptions, and results

This case study was conducted using a simulation-based approach that integrates both empirical data and theoretical assumptions. The reliance on this approach, while valuable, inherently introduces uncertainties into the predicted outcomes, challenging the robustness of the findings. The potential limitations in the method, assumptions, and results of this study are summarized as follows.

The historical data for grid electricity emission factors reflects the current status in the Netherlands, but it is important to note that this factor is subject to significant variation in the coming decades due to political, economic, and environmental factors. In a possible future

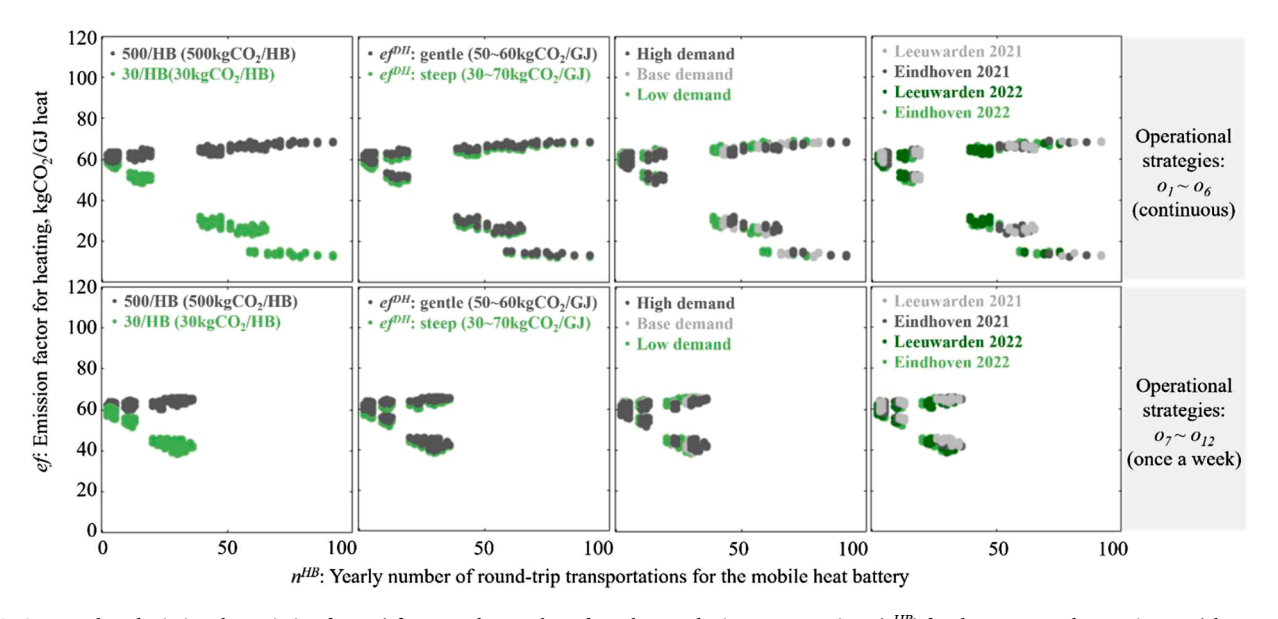


Fig. 16. Scatter plots depicting the emission factor (*ef*) versus the number of yearly round-trip transportations (n^{HB}) for the M-HB, under continuous (above, $o_1 \sim o_6$) and weekly (below, $o_7 \sim o_{12}$) supply strategies. Points are color-coded to represent the different scenarios.

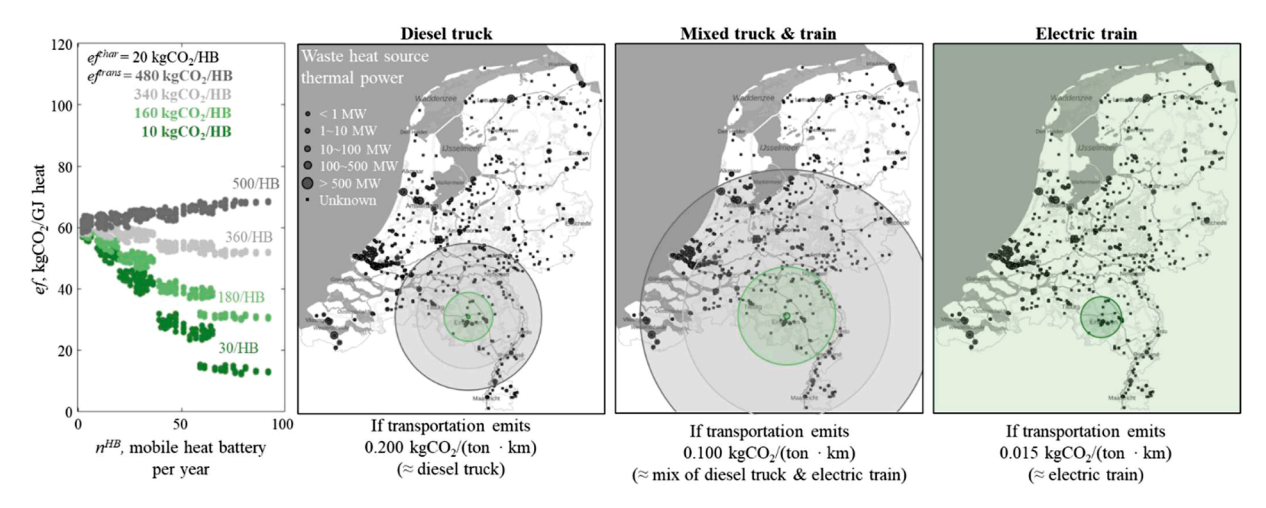


Fig. 17. Heating emission factor ef and waste heat harvest circles in different scenarios.

scenario, more renewable energy may be incorporated into the grid, and the decarbonization potential of the M-HB system might decrease since the benchmark system can already utilize low-emission electricity. Given the dynamic nature of energy landscapes, it's imperative to incorporate various grid decarbonization scenarios into future analyses to assess their impact on the efficacy of M-HB systems. Nevertheless, the M-HB's flexibility allows for adaptive strategies in response to shifts in the energy landscape. For instance, it can be utilized to mitigate grid congestion resulting from peak periods of renewable energy production.

The "gentle" and "steep" scenarios for DH emissions may not capture the full range of possibilities, and actual emissions can vary per system. But in a DH system with low or zero emissions, the role of a M-HB may transition to serving as a peak or backup heat source. The case study demonstrates this potential by showing how the M-HB, with its 100 kW thermal output, can temporarily replace the heat supply from DH and local electricity grids.

While the models utilized have undergone validation through various methods, it's critical to continuously assess and refine them to minimize the potential for predictive inaccuracies that could compromise the integrity of the results. For instance, a 1 % error in predicting the heat battery's discharge *COP* could result in a similar margin of error in the electrical energy consumed during discharge, potentially affecting the decarbonization potential estimates. To mitigate such impacts, this study has focused on maintaining an acceptable accuracy index.

6.2. Brief comparison with other alternatives

This study juxtaposes the established heating framework of a neighborhood with a novel setup that incorporates a M-HB. It is important to note that these are not the only two options available; a variety of alternative waste heat transport methods and comprehensive heating solutions exist for consideration. A comparative analysis of all these systems is out of the scope of this paper. However, below a short discussion is provided.

While this study focuses on the integration of M-HBs, it's essential to acknowledge alternative waste heat transport methods and heating solutions. Sensible and latent heat storage technologies, for instance, offer distinct advantages such as rapid discharge capabilities but are plagued by significant storage losses and limited energy density. In our case study, the duration between two discharging signals to the heat battery can be very long. For instance, as shown in Fig. 12, a storage capacity of 10 GJ was depleted over an entire month, which is impossible for those TES systems with significant storage loss. Moreover, the high energy density of the M-HB results in fewer than 100 transportation events annually in this scenario, a figure that could increase with alternatives possessing lower energy densities, potentially leading to greater

disturbance within the neighborhood.

The neighborhood under study also has access to other heating options, including distributed air-to-water heat pumps, gas boilers, or centralized DH systems. Preliminary calculations suggest that an air-to-water heat pump with a COP of 3 and an ef^{elec} of $100~{\rm KgCO_2/MWh}$ could have an ef of approximately 120 KgCO₂/GJ—twice that of the benchmark system. A gas boiler, with a 90 % conversion efficiency, might yield an ef of about 63 KgCO₂/GJ, which aligns closely with the benchmark and therefore is generally higher than the system integrating a heat battery. DH systems, as exemplified in Fig. 1, would benefit more from the direct utilization of clean energy sources in low-emission configurations such as the systems at the bottom-left corner in Fig. 1 with ef^{OH} values lower than 30 KgCO₂/GJ., while higher-emission systems could see improvements through the integration of the heat battery, especially for those at the top-right corner in Fig. 1 with ef^{OH} values higher than 80 KgCO₂/GJ.

7. Conclusion

This study embarks on a comprehensive evaluation of the decarbonization potential of M-HBs in low-temperature DH systems, based on theoretical assumptions and empirical data in the context of the Netherlands. The research methodology centers around an analysis of the system's operational carbon emissions (per GJ delivered heat) from consuming grid electricity, consuming heat from DH, plus the emissions from transport and charging of the M-HB. The key findings include:

Broad Decarbonization Potential: The utilization of M-HBs demonstrates a remarkable potential for slashing carbon emissions, with scenarios revealing staggering reductions of up to 80 % from initial levels of 60 to 70 KgCO₂/GJ down to a mere 13 KgCO₂/GJ.

Strategic Operational Efficiency: This study underscores the strategic efficiency of specific operational strategies, particularly those ensuring continuous waste heat supply $(o_1, o_2, \text{ and } o_4)$ in the 30/HB scenario, suggesting promising avenues for substantial emission reductions. However, the variability in impact highlights the critical importance of carefully considering M-HB charging and transportation mechanisms.

Waste Heat Harvest Circle Insights: The examination of the waste heat harvest circle offers crucial insights into the practicality of waste heat recovery. From the limited reach observed in the 30/HB scenario using diesel trucks to the extensive range enabled by a combination of electric trains and trucks, transportation methods and emission factors emerge as pivotal determinants.

The significance of this research lies in its contribution to understanding how M-HBs can be used in the transformation to more sustainable DH systems. It paves the way for further research, including broader analyses of waste heat utilization and economic-environmental impacts. Future investigations could delve into broader analyses of waste heat utilization, economic-environmental impacts, and integration with diverse urban infrastructures and renewable energy sources. Exploring the scalability and long-term effects of M-HBs, alongside their implications for urban energy policies and infrastructure development, promises invaluable insights for fostering sustainable urban environments.

CRediT authorship contribution statement

Shuwei Wang: Writing – original draft, Visualization, Validation, Software, Methodology, Conceptualization. **Pieter-Jan Hoes:** Writing – review & editing, Validation, Supervision, Methodology, Conceptualization. **Jan L.M. Hensen:** Writing – review & editing, Validation, Supervision, Methodology, Conceptualization. **Olaf C.G. Adan:** Writing – review & editing, Validation, Supervision, Resources.

Declaration of competing interest

The authors declare that they have no known competing financial interests or personal relationships that could have appeared to influence the work reported in this paper.

Data availability

Data will be made available on request.

Acknowledgements

This research has been supported by project 9.4: development of closed-loop TCM system, which is part of the 'Integrale Energietransitie Bestaande Bouw' (IEBB). The IEBB project was initiated by the Building and Technology Innovation Centre (BTIC) and is funded by Rijksdienst voor Ondernemend (RVO) Nederland. The authors express sincere appreciation to Pim A.J. Donkers and Jan van Dorst for their support in information and resources for this research.

References

- Averfalk, H. ;, Werner, S. ;, Felsmann, C. ;, Rühling, K. ;, Wiltshire, R. ;, & Svendsen, S. (2023). Transformation Roadmap from High to Low Temperature District Heating Systems Annex XI final report.
- Bennici, S., Dutournié, P., Cathalan, J., Zbair, M., Nguyen, M. H., Scuiller, E., & Vaulot, C. (2022). Heat storage: Hydration investigation of MgSO4/active carbon composites, from material development to domestic applications scenarios. Renewable and Sustainable Energy Reviews, 158, Article 112197. https://doi.org/10.1016/J. RSER.2022.112197
- Blokker, M., Agudelo-Vera, C., Moerman, A., Van Thienen, P., & Pieterse-Quirijns, I. (2017). Review of applications for SIMDEUM, a stochastic drinking water demand model with a small temporal and spatial scale. *Drinking Water Engineering and Science*, 10(1), 1–12. https://doi.org/10.5194/DWES-10-1-2017
- Boris van Beijnum, & Ruud van den Wijngaart. (2023). Referentieverbruik warmte woningen achtergrondrapport. https://www.pbl.nl/sites/default/files/downloads/pbl-2023-referentieverbruik-warmte-woningen-achtergrondrapport_5168.pdf.
- Cellcius B.V. (2023). Cellcius homepage. https://cellcius.com/en/.
- Du, K., Calautit, J., Eames, P., & Wu, Y. (2021). A state-of-the-art review of the application of phase change materials (PCM) in Mobilized-Thermal Energy Storage (M-TES) for recovering low-temperature industrial waste heat (IWH) for distributed heat supply. Renewable Energy, 168, 1040–1057. https://doi.org/10.1016/J. RENEWE.2020.12.057
- Elci, M., Manrique Delgado, B., Henning, H. M., Henze, G. P., & Herkel, S. (2018). Aggregation of residential buildings for thermal building simulations on an urban district scale. Sustainable Cities and Society, 39, 537–547. https://doi.org/10.1016/J. SCS.2018.03.015
- $Eneco.\ (2023).\ \textit{Warmte-etiket}.\ https://www.eneco.nl/warmte-etiket/.$
- Ennatuurlijk. (2023). Warmte-etiketten. https://ennatuurlijk.nl/thuis/warmte-en-kou de/warmte-etiket-ennatuurlijk.
- European Commission. (2023). ETS2: Buildings, road transport and additional sectors. https://climate.ec.europa.eu/eu-action/eu-emissions-trading-system-eu-ets/ets2-buildings-road-transport-and-additional-sectors_en#documentation.

- Gautam, A., & Saini, R. P. (2020). A review on technical, applications and economic aspect of packed bed solar thermal energy storage system. *Journal of Energy Storage*, 27, Article 101046. https://doi.org/10.1016/J.EST.2019.101046
- Guelpa, E., & Verda, V. (2019). Thermal energy storage in district heating and cooling systems: A review. Applied Energy, 252, Article 113474. https://doi.org/10.1016/J. APENERGY.2019.113474
- Guo, S., Zhao, J., Bertrand, A., & Yan, J. (2022). Mobilized thermal energy storage for clean heating in carbon neutrality era: A perspective on policies in China. *Energy and Buildings*, 277, Article 112537. https://doi.org/10.1016/J.ENBUILD.2022.112537
- IEA. (2022). Heating degree days in the Netherlands, 2000-2020 charts data & statistics. https://www.iea.org/data-and-statistics/charts/heating-degree-days-in-the-netherlands-2000-2020
- Johari, F., Shadram, F., & Widén, J. (2023). Urban building energy modeling from georeferenced energy performance certificate data: Development, calibration, and validation. Sustainable Cities and Society, 96, Article 104664. https://doi.org/ 10.1016/J.SCS.2023.104664
- Jokinen, I., Lund, A., Hirvonen, J., Jokisalo, J., Kosonen, R., & Lehtonen, M. (2022). Coupling of the electricity and district heat generation sectors with building stock energy retrofits as a measure to reduce carbon emissions. *Energy Conversion and Management*, 269, Article 115961. https://doi.org/10.1016/J. ENCONMAN.2022.115961
- Ju, Y., Jokisalo, J., & Kosonen, R. (2023). Peak shaving of a district heated office building with short-term thermal energy storage in Finland. *Buildings 2023*, 13(3), 573. https://doi.org/10.3390/BUILDINGS13030573. Vol. 13, Page573.
- Kant, K., & Pitchumani, R. (2022). Advances and opportunities in thermochemical heat storage systems for buildings applications. *Applied Energy*, 321, Article 119299. https://doi.org/10.1016/J.APENERGY.2022.119299
- Klein, A., Hilster, D., Scholten, P., Van Wijngaarden, L., Tol, E., & Otten, M. (2021). STREAM Goederenvervoer 2020 Emissies van modaliteiten in het goederenvervoer-Versie 2. https://ce.nl/wp-content/uploads/2021/03/CE_Delft_190325_STREAM_Goedervervoer_2020_DEF_Versie2.pdf.
- Koninklijk Nederlands Meteorologisch Instituut KNMI. (2023). Hourly values of weather stations. https://daggegevens.knmi.nl/klimatologie/uurgegevens.
- Kuang, R., Huang, N., Chen, G., Tan, J., Liu, J., & Shen, Y. (2022). Numerical analysis of discharging stability of basalt fiber bundle thermal energy storage tank. *Energy Reports*, 8, 13014–13022. https://doi.org/10.1016/J.EGYR.2022.09.115
- Liu, Z., Liu, Z., Guo, J., Wang, F., Yang, X., & Yan, J. (2022). Innovative ladder-shaped fin design on a latent heat storage device for waste heat recovery. *Applied Energy*, 321, Article 119300. https://doi.org/10.1016/J.APENERGY.2022.119300
- Loonen, R. C. G. M., de Klijn-Chevalerias, M. L., & Hensen, J. L. M. (2019). Opportunities and pitfalls of using building performance simulation in explorative R&D contexts. *Journal of Building Performance Simulation*, 12(3), 272–288. https://doi.org/ 10.1080/19401493.2018.1561754
- Lund, H., Werner, S., Wiltshire, R., Svendsen, S., Thorsen, J. E., Hvelplund, F., & Mathiesen, B. V. (2014). 4th Generation District Heating (4GDH): Integrating smart thermal grids into future sustainable energy systems. *Energy*, 68, 1–11. https://doi. org/10.1016/J.ENERGY.2014.02.089
- Maximov, S. A., Mehmood, S., & Friedrich, D. (2021). Multi-objective optimisation of a solar district heating network with seasonal storage for conditions in cities of southern Chile. Sustainable Cities and Society, 73, Article 103087. https://doi.org/ 10.1016/J.SCS.2021.103087
- Ministerie van Binnenlandse Zaken en Koninkrijksrelaties. (2014). WoonOnderzoek Nederland 2012 - module Energie. https://open.overheid.nl/Details/ronl-archief-e0ef d368-35b4-44b8-b357-a51bbc9f931d/1.
- Ministerie van Binnenlandse Zaken en Koninkrijksrelaties (BZK), & Centraal Bureau voor de Statistiek (CBS). (2019). WoON2018energie: Release 1.0 – Energiemodule WoON2018.
- Miró, L., Gasia, J., & Cabeza, L. F. (2016). Thermal energy storage (TES) for industrial waste heat (IWH) recovery: A review. Applied Energy, 179, 284–301. https://doi.org/ 10.1016/J.APENERGY.2016.06.147
- Municipality of Eindhoven. (2023). Natural-gas-free Northeast. https://www.eindhovend uurzaam.nl/energie-warmte/aardgasvrij/aardgasvrij-noordoost.
- NEN. (2017, June 1). NEN 7125:2017 (nl) Energieprestatienorm voor maatregelen op gebiedsniveau (EMG) Bepalingsmethode. https://www.nen.nl/nen-7125-2017-nl-
- NEN. (2023). NTA 8800:2023 (nl) Energieprestatie van gebouwen Bepalingsmethode. NetAnders. (2023). CO2 Monitor. https://co2monitor.nl/en.
- Pan, Y., Zhu, M., Lv, Y., Yang, Y., Liang, Y., Yin, R., & Yuan, X. (2023). Building energy simulation and its application for building performance optimization: A review of methods, tools, and case studies. *Advances in Applied Energy*, 10, Article 100135. https://doi.org/10.1016/J.ADAPEN.2023.100135
- Pans, M. A., Claudio, G., & Eames, P. C. (2024). Theoretical cost and energy optimisation of a 4th generation net-zero district heating system with different thermal energy storage technologies. Sustainable Cities and Society, 100, Article 105064. https://doi. org/10.1016/J.SCS.2023.105064
- Parra, D., Swierczynski, M., Stroe, D. I., Norman, S. A., Abdon, A., Worlitschek, J., & Patel, M. K. (2017). An interdisciplinary review of energy storage for communities: Challenges and perspectives. *Renewable and Sustainable Energy Reviews*, 79, 730–749. https://doi.org/10.1016/J.RSER.2017.05.003
- Rijksdienst voor Ondernemend Nederland RvO. (2023). Warmte Atlas. https://www.warmteatlas.nl/viewer/app/Warmteatlas/v2.
- Rouhani, M., Huttema, W., & Bahrami, M. (2019). Thermal conductivity of AQSOA FAM-Z02 packed bed adsorbers in open and closed adsorption thermal energy storage systems. *International Journal of Refrigeration*, 105, 158–168. https://doi.org/ 10.1016/J.IJREFRIG.2018.05.012

- Ruiz, G. R., & Bandera, C. F. (2017). Validation of calibrated energy models: Common errors. Energies, 10(10). https://doi.org/10.3390/en10101587
- Siddiqui, S., Macadam, J., & Barrett, M. (2021). The operation of district heating with heat pumps and thermal energy storage in a zero-emission scenario. *Energy Reports*, 7, 176–183. https://doi.org/10.1016/J.EGYR.2021.08.157
- Statistics Netherlands CBS. (2023a). CBS in uw buurt. https://cbsinuwbuurt.nl/#.
- Statistics Netherlands CBS. (2023b). StatLine Stock of homes; average surface area; home type, year of construction, region. https://opendata.cbs.nl/#/CBS/nl/dataset/82550 NED/table?ts=1700224603323.
- Swanson, D. A. (2015). On the relationship among values of the same summary measure of error when it is used across multiple characteristics at the same point in time: An examination of MALPE and MAPE. *Review of Economics & Finance, 5*(1), 1–14. ISSN (p) 1923-7529, ISSN(e) 1923-8401 https://escholarship.org/uc/item/1f71t3x9.
- Vattenfall. (2023). Warmte-etiket met onze warmtebronnen. https://www.vattenfall.nl/st adsverwarming/warmte-etiket/.
- Wang, S., Hoes, P. J., Hensen, J. L. M., Adan, O. C. G., & Donkers, P. A. J. (2023a). A design optimization method for solar-driven thermochemical storage systems based on building performance simulation. *Journal of Energy Storage*, 72, Article 108354. https://doi.org/10.1016/J.EST.2023.108354

- Wang, S., Hoes, P. J., Hensen, J. L. M., Adan, O. C. G., & Donkers, P. A. J. (2023b). Investigating the use cases of a novel heat battery in Dutch residential buildings. *Building Simulation*, 16(9), 1675–1689. https://doi.org/10.1007/S12273-023-1069-2/METRICS
- Woonbedrijf, & BAM Wonen. (2021). Renovatie generalenbuurt zuid. https://www.woonbedrijf.com/Media/ae26c386-c33e-4b3c-bfa0-f9c06a4aae37/original/infoboekje-generalenbuurt-zuid-fase-1.pdf/.
- Xu, J. X., Li, T. X., Chao, J. W., Yan, T. S., & Wang, R. Z. (2019). High energy-density multi-form thermochemical energy storage based on multi-step sorption processes. *Energy*, 185, 1131–1142. https://doi.org/10.1016/J.ENERGY.2019.07.076
- Yan, T., & Zhang, H. (2022). A critical review of salt hydrates as thermochemical sorption heat storage materials: Thermophysical properties and reaction kinetics. Solar Energy, 242, 157–183. https://doi.org/10.1016/J.SOLENER.2022.07.002
- Zeng, Z., Zhao, B., & Wang, R. (2023). Water based adsorption thermal battery: Sorption mechanisms and applications. *Energy Storage Materials*, 54, 794–821. https://doi. org/10.1016/J.ENSM.2022.11.024
- Zhou, Y., & Liu, Z. (2023). A cross-scale 'material-component-system' framework for transition towards zero-carbon buildings and districts with low, medium and hightemperature phase change materials. Sustainable Cities and Society, 89, Article 104378. https://doi.org/10.1016/J.SCS.2022.104378